Journal of Applied Polymer Science

Complex aggregates formed with a hyperbranched polyglycerol derivative for drug delivery

Qianqian Zheng,[1] Xiaoyan Zhou,[1] Hui Li,[1] Dong Ma,[1] Wei Xue[1,2]

[1]Key Laboratory of Biomaterials of Guangdong Higher Education Institutes, Department of Biomedical Engineering, Jinan University, Guangzhou 510632, China

[2]Institute of Life and Health Engineering, Key Laboratory of Functional Protein Research of Guangdong Higher Education Institutes, Jinan University, Guangzhou 510632, China

Correspondence to: D. Ma (E-mail: madong_jnu@163.com) and W. Xue (E-mail: weixue_jnu@aliyun.com.cn)

ABSTRACT: An amphiphilic hyperbranched polyglycerol derivative (HPG-C18) was synthesized by the anionic ring-opening copolymerization with glycidol and 1,2-epoxyloctadecane as the monomers. This hyperbranched polymer formed large complex aggregates as confirmed by dynamic light scattering and transmission electron microscopy tests. Because of its amphiphilic properties, HPG-C18 was explored to load hydrophobic docetaxel, a clinical antitumor drug, and deliver it into breast cancer cell line (MCF-7) cells. To investigate the application of the aggregates in drug delivery, blood compatibility was studied by hemolysis analysis, red blood cell observation, and thromboelastography assay. These results indicate that HPG-C18 inhibited MCF-7 proliferation effectively with good blood compatibility, and this suggested a potential application in tumor therapy. © 2015 Wiley Periodicals, Inc. J. Appl. Polym. Sci. **2016**, *133*, 42895.

KEYWORDS: biocompatibility; drug-delivery systems; micelles

Received 3 May 2015; accepted 27 August 2015
DOI: 10.1002/app.42895

INTRODUCTION

Nanoparticles have attracted much attention in biomedicine because of their nanometer size and good stability. For examples, micelles self-assembled from amphiphilic block copolymers have played an important role in drug delivery because they can solubilize hydrophobic drugs, decline side effects, and improve the bioavailability.[1–5] Micelles can be classified as simple and complex micelles according to their structure and size. Simple micelles are formed by the primary aggregation of amphiphilic block copolymers because of microphase separation; they have an aggregated structure, as shown in Scheme 1. Thus, they were called *primary micelles* by Eisenberg *et al.*[6] and are usually smaller than 20 nm. Complex micelles are more complicated in structure and larger in size (usually >100 nm), and they have attracted a lot of attention from both academia and industry because of their superior stability and controlled drug release.[7,8]

Zhang *et al.*[9] studied several large crew-cut micelles self-assembled by linear block copolymers. It was pointed out that the complex micelles were formed by the secondary aggregation of primary micelles or reverse micelles. Liu *et al.*[10] prepared the amphiphilic dendritic star-block copolymer complex micelles with pH response and used them to deliver camptothecine into Hela cells. Radowski *et al.*[11] synthesized an amphiphilic dendritic block copolymer and prepared complex nanocarriers through supramolecular aggregation. We found that the nanocarriers self-assembled into supramolecular aggregates above a well-defined threshold concentration.

Among the polymers used to construct micelle nanoparticles, hyperbranched polyglycerol derivatives (HPG) have been emerged as a new type of candidate for solution self-assembly. These polymers often form unimolecular micelles because of their unique topologies; these include highly branched structures and spherical shapes, which are important for drug delivery.[12] Unimolecular micelles usually show good stability in aqueous solution, even at low concentrations. They can prevent drug leakage effectively and enhance bioavailability during blood circulation;[13] this leads to effective drug delivery and disease therapy. Moreover, drug-loaded micelles can be easily accumulated in tumors because of the enhanced permeability and retention (EPR) effect *in vivo*.[14]

In this study, a hyperbranched amphiphilic polyglycerol derivative (HPG) was synthesized and used for drug delivery. It has been reported that HPGs could form stable unimolecular micelles because of their unique topologies.[15,16] HPGs also show excellent blood compatibility and have, therefore, been applied widely in biomedicine.[17,18] In our previous study,[19] we prepared

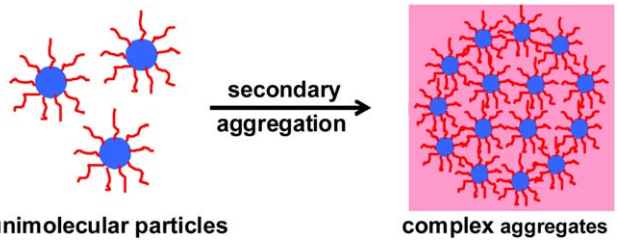

Scheme 1. Formation of large complex aggregates by the secondary aggregation of unimolecular particles. [Color figure can be viewed in the online issue, which is available at wileyonlinelibrary.com.]

a poly(ethylene glycol)–polycaprolactone-modified HPG (HPG-PCL-PEG) polymer and used it to deliver drugs for tumor therapy. However, the obtained HPG–PCL–PEG could not form stable unimolecular micelles. Moreover, the synthesis route of HPG–PCL–PEG was multistep. Herein, the amphiphilic octadecane (C18)-modified HPG was synthesized through a one-pot reaction. As observed, the obtained HPG (HPG-C18) formed unimolecular particles and then further aggregated to large aggregates in aqueous solution; these were formed by the secondary aggregation of the unimolecular particles. The hydrophobic antitumor drug docetaxel (DTX) was loaded into the aggregates to be delivered for breast cancer cell line (MCF-7) tumor cell inhibition. For injectable drug-delivery system, there have been a few reports on their blood compatibility.[20] So, we evaluated the blood compatibility of the aggregates through a hemolysis test, red blood cell (RBC) observation, and thromboelastography (TEG) assay.

EXPERIMENTAL

Materials

Glycidol (96%) was purchased from Aladdin Industrial Corp. (Shanghai, China) and distilled *in vacuo* before use. 1,1,1-Tris(hydroxymethyl) propane (TMP; 99%) was obtained from Adamas Reagent Corp. and was used after it was dried *in vacuo* at 45°C for 12 h. Potassium methylate solution in methanol was purchased from Sigma-Aldrich. 1,2-Epoxyloctadecane was obtained from Tokyo Chemical Industry Corp., Ltd. (Tokyo, Japan) and was used after it was dried *in vacuo* at 45°C for 12 h. Pyrene (98%) and DTX (99%) were purchased from Aladdin Industrial Corp. (Shanghai, China). The MCF-7 cells were obtained from Military Hospital in Guangzhou. Dulbecco's modified Eagle's medium and fetal bovine serum were purchased from Invitrogen Corp. (Washington, DC). A Cell Counting Kit 8 (CCK-8) was purchased from Beyotime Institute of Biotechnology (Shanghai, China). All of the other reagents were of analytical grade from Guangzhou Chemical Reagent (China) and were used as received.

Synthesis of HPGs (HPG-C18)

The HPG-C18 was synthesized according to the reported method.[21] In a typical procedure, TMP (170 mg) was added to a two-necked round-bottomed flask and dried *in vacuo* at 45°C for 12 h. Then, 0.12 mL of potassium methylate solution in methanol (25%) was added to the flask under a nitrogen atmosphere as the partially deprotonated solvent for TMP. The mixture was stirred for 10 min, and then, the excess methanol was removed *in vacuo*. Next, under a nitrogen atmosphere, 12 mL of fresh glycidol was added dropwise at a rate of 0.8 mL/h by a microinjection pump. The flask was kept in an oil bath at 95°C to start the reaction. Under stirring and a nitrogen atmosphere, the reaction lasted for 5 h. Then, 1,2-epoxyoctadecane (3.0 g) was added, and the mixture was stirred for another 24 h. After the reaction, the product was dissolved in methanol and mixed with the cationic exchange resin activated by 2 mol/L hydrochloric acid. The unreacted 1,2-epoxyoctadecane was removed by extraction with hexane, and methanol was removed by rotary evaporation. The resulting HPG-C18 was dialyzed in distilled water for 3 days with a cellulose dialysis bag (molecular weight cutoff = 3000) and frozen to dry.

The chemical structure of HPG-C18 was determined by ^{1}H-NMR at room temperature with hexadeuterated dimethyl sulfoxide (DMSO-d_6) as the solvent. Its molecular weight and polydispersity were determined by gel permeation chromatography (GPC; Malvern, United Kingdom) equipped with a VE 1122 high performance liquid chromatography (HPLC) pump and a model 270 detector. The GPC analysis was performed in water at 35°C with an elution rate of 1 mL/min (with PEO as the standard). The critical aggregation concentration (CAC) of HPG-C18 in an aqueous solution was determined by fluorescence spectroscopy with pyrene as a probe.[22] The fluorescence spectrum was recorded with a fluorescent spectrometer F-7000 (Hitachi, Japan). The emission spectra ranged from 350 to 450 nm with the excitation spectrum fixed at 334 nm, and the emission and excitation slit widths were 2.5 and 5 nm with a scanning speed of 300 nm/min.

DTX Loading and Release

With a dialysis method,[23] a typical procedure for the preparation of DTX-loaded HPG-C18 aggregates in aqueous solution was as follows. HPG-C18 (100 mg) and DTX (10 mg) were dissolved in 5.0 mL of dimethylformamide under stirring; then, 3 mL of deionized water was added dropwise. After the mixture was stirred for 12 h at room temperature, the resulting solution was transferred into a dialysis bag (molecular weight cutoff = 500) against deionized water for 48 h to remove the extra organic solvent. The dialysate was then filtered through a syringe filter (0.45-μm pore size) to remove the unloaded DTX. The DTX-loaded HPG-C18 was obtained after lyophilization.

The loading amount of DTX was determined by HPLC (Agilent 1200). The lyophilized micelles were distilled in methanol at room temperature and then analyzed by an HPLC instrument equipped with a reverse-phase C-18 column (Zorbax Eclipse XDB-C18, 150 × 4.6 mm^2, 5 μm). A mixture of acetonitrile, methanol, and deionized water (40:35:25 v/v) was used as the mobile phase with a flow rate of 1 mL/min. The detection wavelength and column temperature were set at 230 nm and 30°C, respectively. All of the samples were filtered through a syringe filter (0.45-μm pore size) before injection. The standard curve of DTX was made with DTX solutions with concentrations ranging from 2.5 to 50 μg/mL.

The size and ς potential of the HPG-C18 aggregates were measured by dynamic light scattering with a Malvern Instrument (Zetasizer Nano-ZS, Malvern, United Kingdom). Scattered light was collected at a fixed angle of 90°, and all data were averaged

over three measurements. The morphology of the micelles was observed via transmission electron microscopy (TEM; JEM-2010HT, JEOL, Japan). The aqueous HPG-C18 was adjusted to 1.0 mg/mL and stained with 2% w/w phosphotungstic acid for 30 s. We studied the stability of the aggregates monitoring their sizes and ς potentials for 1 week.

For the *in vitro* dual-drug-release assay, 1 mL of DTX-loaded HPG-C18, which was enclosed in the dialysis bag (molecular weight cutoff = 2000) was immersed in 10 mL of phosphate-buffered saline (PBS; 0.01 mol/L, pH 7.4) containing 10% Tween 80 at 37°C. At predetermined time points, 5 mL of the medium solution was taken out, and 5 mL of fresh PBS containing Tween 80 was added back to maintain the same solution volume. The amount of released DTX was determined by HPLC analysis. The cumulative amount of released DTX was calculated from a standard calibration curve. All of the release studies were carried out in triplicate.

In Vitro Cytotoxicity

The cytotoxicity of HPG-C18 and DTX-loaded HPG-C18 was evaluated *in vitro* by CCK-8 assay. MCF-7 cells were first seeded onto a 96-well plate (7×10^3 cells/well) and incubated at 37°C for 12 h. Then, the medium was replaced by fresh medium containing various concentrations of free DTX, DTX-loaded HPG-C18 aggregates (HPG-C18–DTX), and blank HPG-C18, and each sample was set for five wells. The cells were further incubated at 37°C for 24 and 48 h. The cells treated with PBS were incubated under the same conditions and set as the control group. After incubation, the cells were washed with PBS and then incubated in 100 μL of Dulbecco's modified Eagle's medium containing 10 μL of CCK-8 per well for another 2 h. The absorbance in each well was measured at a wavelength of 450 nm by a microplate reader to calculate the number of viable cells.

Blood Compatibility

Hemolysis. For the hemolysis test, fresh whole blood was first obtained from three healthy volunteers by venipuncture with sodium citrate as an anticoagulant, and the volume ratio of blood to sodium citrate was set as 9:1. The obtained whole blood was centrifuged at 1000× g for 5 min. Then, the resulting plasma and buffer coat layer were discarded. The remaining RBC pellets were washed with PBS three times. After that, RBCs were suspended in PBS to form a suspension at 16% v/v hematocrit. Then, 1 mL of HPG-C18 solution at concentrations of 10, 1, 0.1, and 0.01 mg/mL was mixed with 50-μL RBC suspensions, and the mixture was incubated at 37°C for 4 h. RBC suspensions incubated with PBS were used as a control. To induce complete hemolysis, the RBC suspensions were treated with a 0.1% Na_2CO_3 solution for 4 h. After incubation, the RBC suspensions were centrifuged again at 1000 × g for 5 min. A volume of 200 μL of supernatant was taken out to measure their absorbance at 540 nm with a 96-well plate reader (Multiskan MK3; Thermo Lab Systems, Finland). The hemolysis was calculated with the following formula:[24]

$$\text{Hemolysis } (\%) = \frac{A\text{-}B}{C\text{-}B} \times 100$$

where *A*, *B*, and *C* are the absorbances of the test samples, the RBC suspension treated with PBS, and the RBC suspension of complete hemolysis, respectively.

Aggregation and Morphology of RBCs. To observe the morphology of the RBCs, 25 μL of RBCs obtained previously were incubated with 500 μL PBS or aqueous HPG-C18 solutions with different concentrations for 10 min. Then, the mixture was centrifuged gently. The obtained RBCs were fixed by 4% paraformaldehyde overnight at 25°C and then planted onto cleaned glass slides to be dehydrated through immersion of the glass slides into 75, 85, 95, and 100 vol % ethanol for 10 min, respectively. The dried RBCs were coated with gold and observed with a scanning electron microscope (Philips XL-30).

Activated Partial Thromboplastin Time (APTT) and Prothrombin Time (PT). For APTT and PT assays, the platelet-poor plasma was prepared by centrifugation of citrated fresh whole blood at 3000 ×g for 15 min, and then, the resulting supernatant was collected. A volume of 270 μL of collected plasma was then mixed with 30 μL of a PBS or aqueous HPG-C18 solution. The samples were analyzed at 37°C on an SF-8000 automatic coagulation analyzer (Succeeder Co., Beijing, China) with corresponding reagents (provided by the First Affiliated Hospital of Jinan University) added. Each experiment was repeated three times to get a reliable value.

TEG Assays on Blood Coagulation. TEG assays were carried out with a Thromboelastograph Hemostasis System 5000 (TEG) from Haemoscope Corp. at 37°C. The obtained citrated whole blood (900 μL) was mixed with 100 μL of HPG-C18 solution in PBS in a tube contained with kaolin. The sample mixed with 100 μL of PBS was used as a control. Then, the mixture was added to a TEG cup, and the TEG analysis was initiated by the addition of 20 μL of a 0.2 mol/L $CaCl_2$ solution.

Statistical Analysis

A comparison between the groups was analyzed by the one-tailed Student's *t* test with the statistical software SPSS 11.5. All of the data are presented as means and standard deviations. Differences were considered to be statistically significant when the *p* values were less than 0.05.

RESULTS AND DISCUSSION

HPG-C18 Synthesis and DTX Loading

The hyperbranched HPG-C18 was synthesized by the anionic ring-opening polymerization, and the synthetic route is shown in Scheme 2. Its chemical structure was characterized by ^{1}H-NMR and GPC tests. As shown in Figure 1, the ^{1}H-NMR spectrum of HPG-C18 showed the signals of methylene and methane protons of HPG around 3.4 ppm, and the hydroxyl protons were found at 4.6 ppm. The signal at 0.9 ppm was due to the methyl group of the initiator TMP. The continuous methylene protons of C18 alkyl chains responded to the signal at 1.26 ppm. These results demonstrate that the C18 alkyl chains were conjugated to the HPG ending. Through the calculation of the ratio of peak areas of methylene protons from C18 ($\delta = 1.26$ ppm) and methyl protons from the core of HPG ($\delta = 0.9$ ppm), the weight content of C18 in the HPG-C18 conjugate was confirmed as approximately 17.4 wt %. From the GPC trace with PEG as a standard, the weight-average molecular weight (M_w) of HPG-C18 was found to be 9083, and its molecular weight

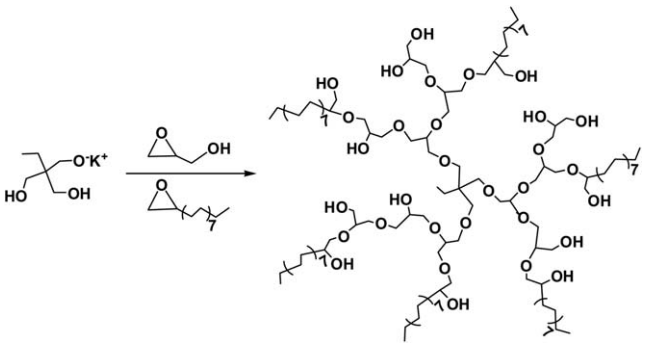

Scheme 2. Synthesis route of HPG-C18.

distribution coefficient (M_w/M_n, where M_n is the number-average molecular weight) was determined to be 1.68.

Similar to most self-assembled micelles formed from amphiphilic polymers, HPG-C18 was also expected to form nanoparticles for drug delivery. We expected that HPG-C18 would form aggregates with the C-18 core and HPG shell, and the driving force for the formation of aggregates was the hydrophobic interactions between C18 segments. It has been reported that amphiphilic HPG derivatives can form unimolecular particles, which have smaller particle sizes compared with normal micelles formed by one molecule. This could be explained by their unique topologies, including their highly branched structures and spherical shapes.[15,16] From dynamic light scattering results, as shown in Figure 2(A), we found that the size of HPG-C18 aggregates was approximately 226.4 nm; these would be better called *large aggregates* rather than unimolecular particles. To explain the reason for the large particle size of HPG-C18 aggregates, TEM observation was carried out. From the TEM observation shown in Figure 2(B), we found that HPG-C18 formed large complex aggregates with a size of 200 nm or so. Interestingly, the TEM image also exhibited fine structures in every large complex aggregate. The amplified image of an aggregate (insert image) clearly indicated that the large aggregates were composed of small spherical building units. The size of the small spherical particles was approximately 8–16 nm; this was

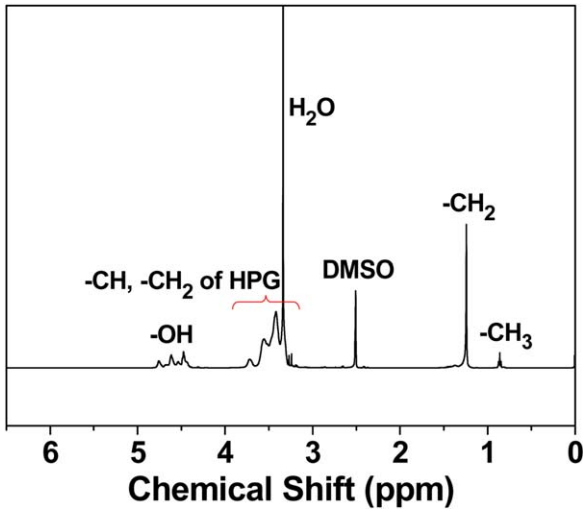

Figure 1. ^{1}H-NMR spectrum of HPG-C18 (DMSO-d_6, 25°C). [Color figure can be viewed in the online issue, which is available at wileyonlinelibrary.com.]

in accordance with that of unimolecular particles. This might have resulted from the aggregation of a large number of unimolecular particles to form complex aggregates. HPG-C18 formed unimolecular particles in aqueous solution because of hydrophobic interactions between C18 segments; then, the unimolecular particles aggregated further. Evidently, the large multimolecular aggregates were built up from the secondary aggregation of unimolecular particles; this was probably related to the hydrophobic interactions between unimolecular particles.[25]

It has been reported that hyperbranched copolymers remain as unimolecular micelles/particles below CAC and, above CAC, they further aggregate together to form large multimolecular aggregates as driven by hydrophobic interactions.[26] In this study, the self-assembling ability of HPG-C18 in aqueous solution was confirmed by CAC measurements with pyrene as a fluorescent probe. Figure 3 shows a typical evolution of the peak intensity of the third peak to the first peak from pyrene (I_3/I_1) ratio as a

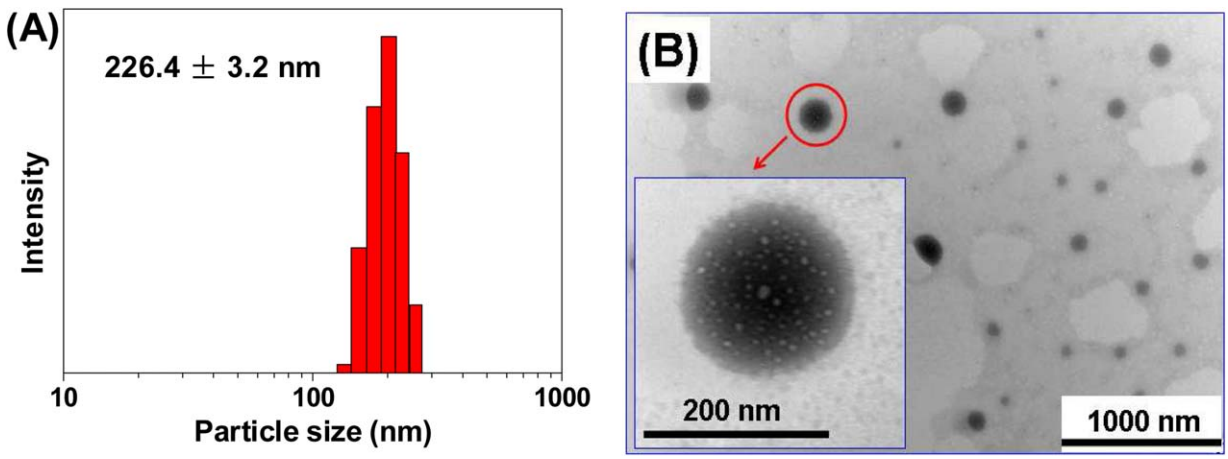

Figure 2. (A) Particle size and (B) TEM image of aqueous HPG-C18 aggregates (HPG-C18 concentration = 5 mg/mL, $n = 3$). [Color figure can be viewed in the online issue, which is available at wileyonlinelibrary.com.]

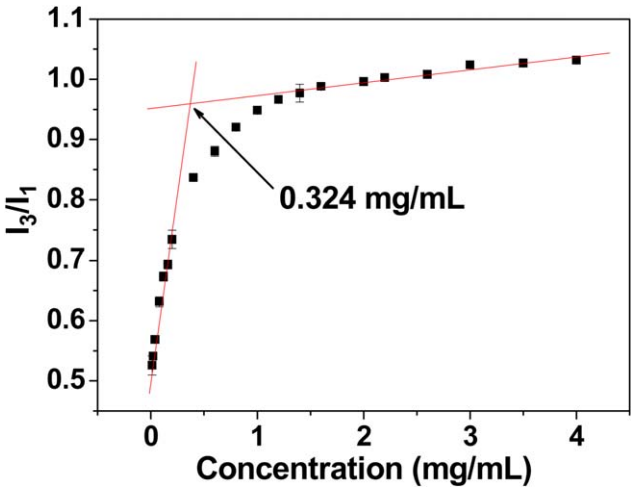

Figure 3. Effect of the HPG-C18 concentration on the I_3/I_1 ratios of pyrene in an aqueous HPG-C18 solution ($n = 3$). [Color figure can be viewed in the online issue, which is available at wileyonlinelibrary.com.]

function of HPG-C18 concentrations in aqueous solution. With increasing HPG-C18 concentration, the intensity ratio exhibited a substantial increase at a certain concentration; this reflected the incorporation of pyrene into the hydrophobic core region of the aggregates. In this case, the CAC value was determined to be 0.324 mg/mL from the crossover point shown in Figure 3. The CAC measurements provided clear evidence for the aggregation process of HPG-C18 in aqueous solution. The copolymers formed unimolecular particles in water below CAC because of the special topology structure of the hyperbranched polymers. Above the CAC, unimolecular particles spontaneously aggregated together to form supramolecular structures; this led to a great increase in the solubility of the fluorescent probes inside the hydrophobic domains of the aggregates.[27]

Because of the low CAC, the obtained amphiphilic HPG-C18 was used to deliver hydrophobic DTX in this study. By HPLC determination, the loading amount of DTX in HPG-C18 was 6.0 mg/g. The stability of HPG-C18–DTX nanoparticles was evaluated by ς potential tests at 37°C for 1 week. As shown in Figure 4, the particle size and ς potential did not significantly change within 1 week, suggesting that HPG-C18–DTX nanoparticles possess an excellent physical stability. The most important advantage of the unimolecular particles was their stability in aqueous solution; this prevented drug leakage effectively when the drug-loaded particles were largely diluted in the blood circulation *in vivo*.[28] Although HPG-C18 formed the complexes aggregates in this study, the complexes aggregates consisted of many unimolecular particles and gave HPG-C18 good stability. So, the obtained HPG-C18–DTX may be an effective system for tumor therapy. Moreover, HPG-C18–DTX showed a negative ς potential; this may have resulted from the abundant oxygen of HPG-C18. The negative charges of HPG-C18–DTX showed better blood stability because of noninteraction with the blood components.

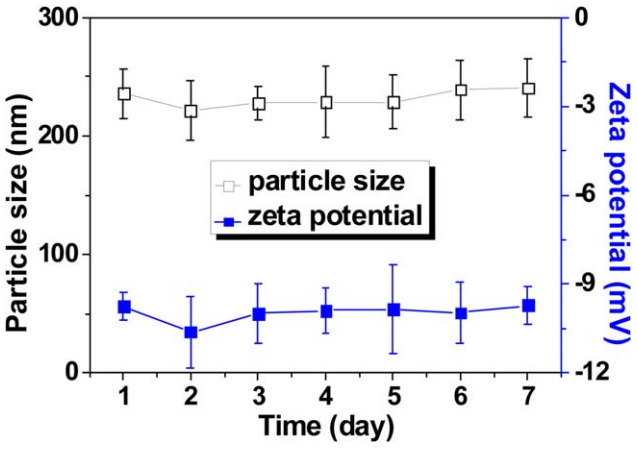

Figure 4. Changes in the particle size and ς potential with time ($n = 3$). [Color figure can be viewed in the online issue, which is available at wileyonlinelibrary.com.]

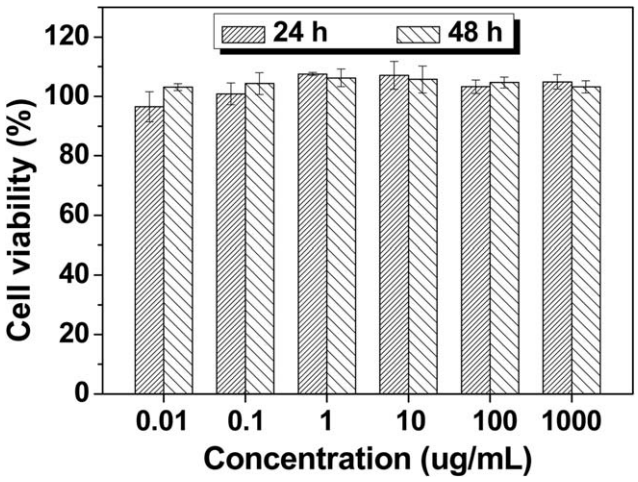

Figure 5. Cytotoxicity results of HPG-C18 for the MCF-7 cells.

Cytotoxicity

The cytotoxicity of the blank HPG-C18 as a drug-delivery system was evaluated first to confirm its safety. The cytotoxicity of HPG-C18 was evaluated on MCF-7 cells by a CCK-8 assay. Figure 5 shows the cell viability results of the MCF-7 cells treated with different HPG-C18 concentrations for 24 and 48 h. As shown, HPG-C18 showed good biocompatibility with MCF-7 cells, and there was no significant difference in the cell viability between PBS and HPG-C18 within the experimental concentrations, even when the HPG-C18 concentration reached 1000 μg/mL.

After DTX was encapsulated, its release behavior was recorded by the immersion of HPG-C18–DTX in PBS medium containing 10% Tween 80. We found that DTX was released quickly in the initial stage and then released slowly after 12 h. After 48 h, approximately 60% loaded DTX was released. This may have been because of the interactions between the carriers and drug, which resulted in the incomplete DTX release from HPG-C18 *in vitro*.[29] However, Figure 6(B) shows the equivalent inhibition effect on MCF-7 cells compared with free DTX; this may have been the reason that DTX was released sequentially after HPG-C18–DTX was released by MCF-7 cells, and also, not all free DTX entered the MCF-7 cells and affected their viability.

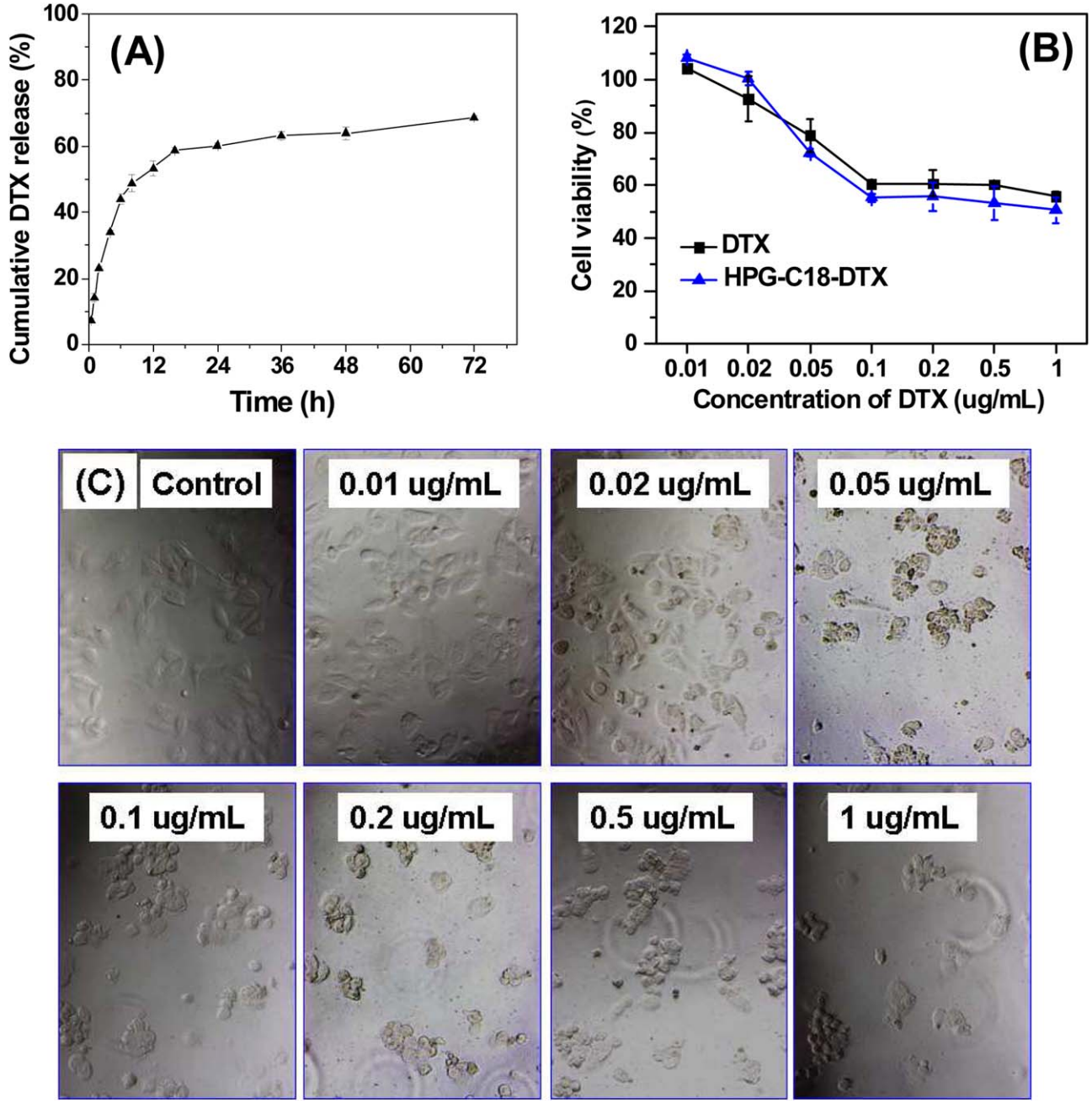

Figure 6. (A) Cumulative DTX release profile from the HPG-C18 aggregates (37°C, $n = 3$). (B) MCF-7 cell viability after incubation with DTX or HPG-C18–DTX at different concentrations for 24 h ($n = 5$, $p < 0.05$). (C) Photographs (10×) of the MCF-7 cells after incubation with HPG-C18–DTX at different concentrations for 24 h. [Color figure can be viewed in the online issue, which is available at wileyonlinelibrary.com.]

The efficiency of HPG-C18–DTX in inhibiting MCF-7 cells was measured by a CCK-8 assay. Figure 6(B,C) shows the cell viability and photographs of MCF-7 cells incubated with HPG-C18–DTX at different concentrations for 24 h. Similar to free DTX used as the control group, the HPG-C18–DTX sample inhibited MCF-7 cell proliferation efficiently, and the inhibition ratio was not significantly different from free DTX. This result indicates that HPG-C18–DTX could enter into the MCF-7 cells easily, and the encapsulation of DTX in HPG-C18 did not hinder the intracellular release of DTX.[30] It has been reported that polymer complexes are usually taken by cells through endocytosis when they are used as drug or gene carries.[31] The amphiphilicity of HPG-C18 made it easily interact with cytomembrane and taken up by cells because of the interactions between the hydrophobic C18 segments and the lipid bilayer of cytomembrane. Moreover, in this experiment, we found that 0.1 μg/mL loaded DTX inhibited 40% MCF-7 cell viability, and the relative HPG-C18 concentration was 167 μg/mL; this was much lower than the safety concentration of 1000 μg/mL. From this result, it was indicated that HPG-C18 could be used as the drug carrier for tumor therapy, although the DTX loading amount was low. The cell morphology, shown in Figure 6(C), also showed that HPG-C18–

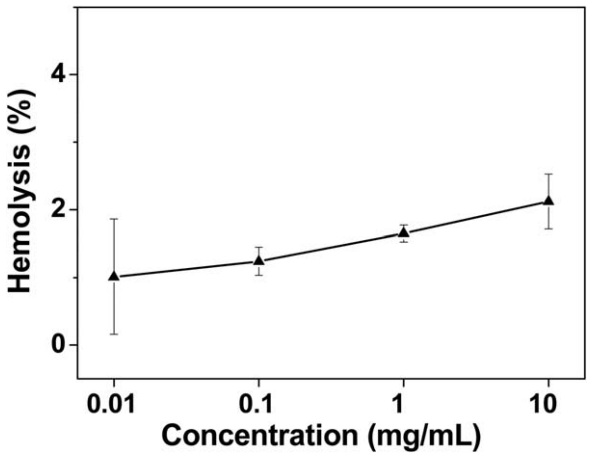

Figure 7. Effect of HPG-C18 with different concentrations on hemolysis ($n = 5$).

DTX inhibited the MCF-7 cell proliferation effectively. With increasing HPG-C18–DTX concentration, the density of the MCF-7 cells decreased, and the cells underwent obvious apoptosis.

Blood Compatibility

The blood compatibility of biomaterials is a key point for considering applications *in vivo*. It has been reported that the instability and nonspecific interactions of nanoparticles in the blood could severely diminish the half-life and bioactivity of loaded drugs and even threaten human life.[32] The blood compatibility of the HPG-C18 nanoparticles was first tested by the spectrophotometric measurement of hemoglobin release from erythrocytes after treatment with different HPG-C18 concentrations. As shown in Figure 7, HPG-C18 displayed good blood compatibility. Even when the concentration was up to 10 mg/mL, HPG-C18 showed nonhemolytic behavior when the extent of hemolysis was lower than the permissible level of 5%.[24]

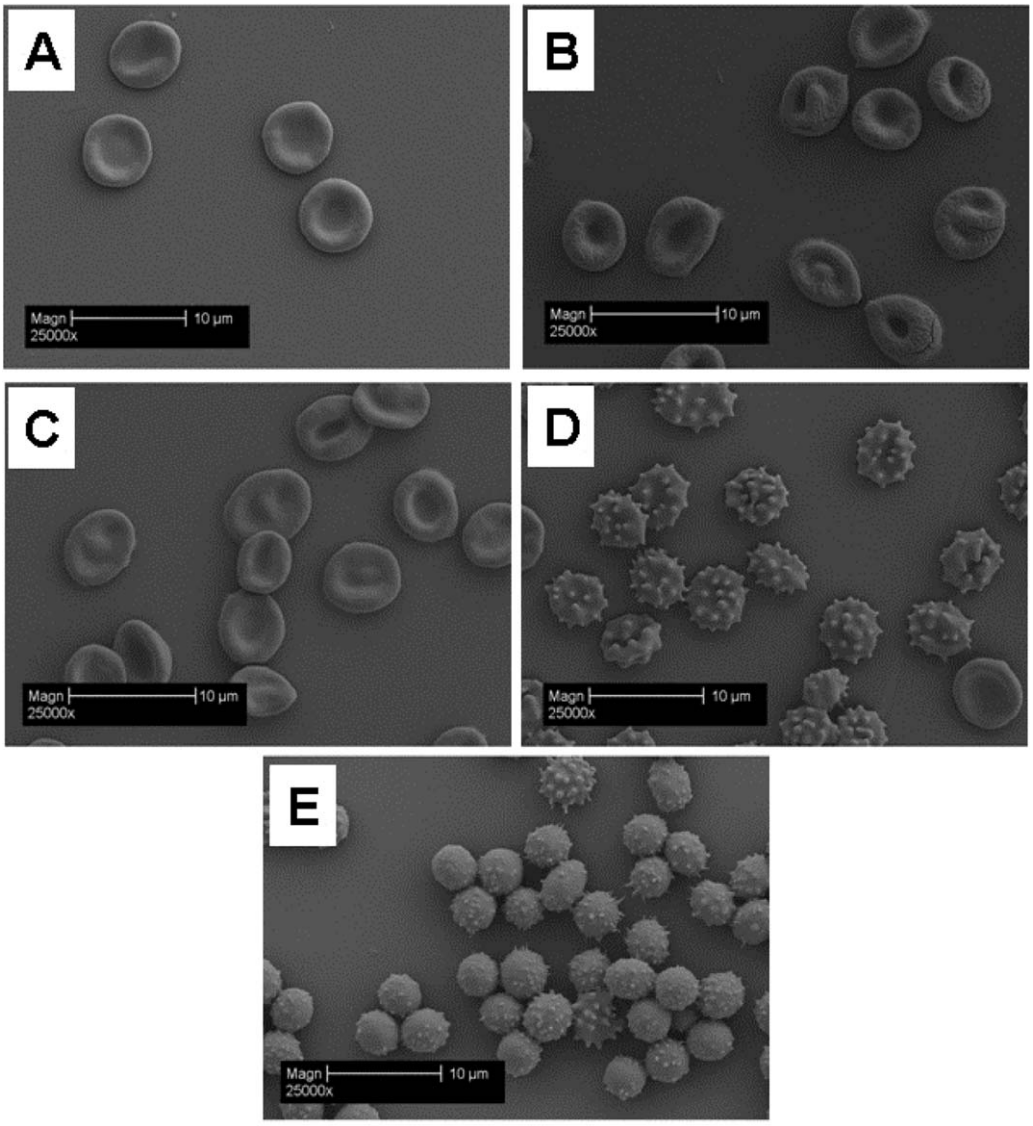

Figure 8. Effect of HPG-C18 on the aggregation and morphology of RBCs: (A) PBS control, (B) 0.01 mg/mL HPG-C18, (C) 0.1 mg/mL HPG-C18, (D) 1 mg/mL HPG-C18, and (E) 10 mg/mL HPG-C18.

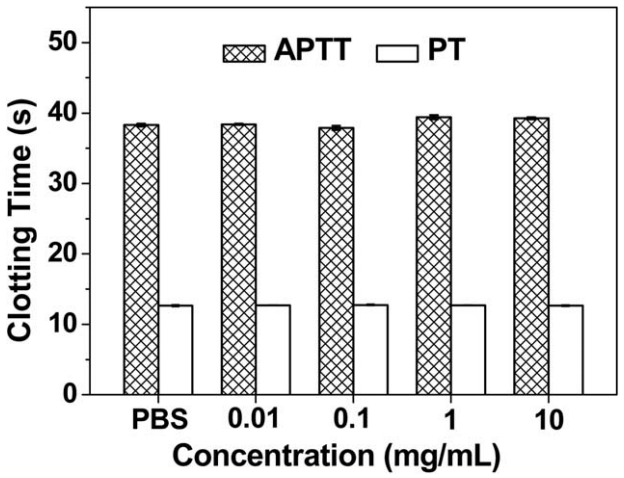

Figure 9. Effect of the HPG-C18 concentration on APTT and PT.

RBCs are abundant in the blood and have a high volume fraction in whole blood (ca. 40–50%), so the interactions between RBCs and nanoparticles must be studied once the administered nanoparticles come into contact with the blood. The effect of HPG-C18 at different concentrations on RBCs aggregation and morphology was studied by scanning electron microscopy observation. As shown in Figure 8, HPG-C18 from 0.01 to 0.1 mg/mL did not cause obvious RBC aggregation or morphological change, and there was no difference in the morphology with PBS control. When the HPG-C18 concentration reached 1 mg/mL, the morphology of the RBCs changed slightly, and the HPG-C18 nanoparticles were adsorbed onto the surface of RBCs and formed a hedgehoglike morphology. According to previous studies,[33] the interaction of RBCs with foreign polymers is mainly driven by electrostatic interactions between the negative RBC surface and the positive polycations and/or by the hydrophobic interaction between the hydrophobic groups of amphiphilic polymers and the lipid bilayer of the RBC membrane. It has been reported that cationic polymers easily cause RBCs to aggregate and fully change their shape to gather together.[34] On the contrary, the negative surface and amphiphilic properties of HPG-C18 in this study resulted in fewer effects on the RBC aggregation and morphology. Moreover, the negative surface eliminated HPG-C18 interactions with proteins of the blood; this also contributed to the good blood compatibility of HPG-C18 in hemolysis and other assays.

APTT and PT assays were also carried out to further detect the abnormality of the blood plasma.[35] The blood coagulation cascade contained three pathways: the intrinsic, extrinsic, and common pathways. APTT indicated the performance of the intrinsic and common coagulation pathways; this gave the time required to form a fibrin clot after a partial thromboplastin reagent was added. PT measured the performance of the extrinsic and common coagulation pathways, and this gave the time to form a fibrin clot after tissue thromboplastin was added. The results of the HPG-C18 concentration affecting APTT and PT are shown in Figure 9. We found that HPG-C18 showed no significant difference in APTT or PT from the PBS control; this indicated no interactions with the coagulation factors and/or thromboplastin reagent. These results demonstrate that HPG-C18 had little effect on the extrinsic route of blood coagulation and showed good blood compatibility.

It has been reported that APTT and PT cannot always accurately reflect the foreign-material-induced anticoagulant activity,[36] so TEG tests were further carried out to provide the details of the blood clotting in this study. TEG characterizes the formation and strength of the blood clot as a function of time and reflects some principle parameters in the blood-clotting process: (1) the reaction time (R), which is the time to reach a 2-mm amplitude in the tracing and which is the time from the initiation of the test to the initial fibrin formation; (2) coagulation time (K), which is the time from 2- to 20-mm amplitude of the tracing and which represents the dynamics of clot formation; (3) α angle, which is the slope of the tangent joining the point of the 2-mm split intercepting the tracing and which is the rate of clot aggregation or fibrin crosslinking; and (4) maximum amplitude (MA) of the tracing, which represents the maximum clot strength.[37] Here, the influence of HPG-C18 on the whole blood-clotting process was measured, and the principle TEG data are listed in Table I. Moreover, the representative TEG traces are also given in Figure 10, which shows the clot formation in PBS and HPG-C18 in a concentration range of 0.01–10 mg/mL. As shown, the initial straight line is the tracing for a period time for all of the samples. At the end of the plateaus, all of the traces deviated into two curves. The amplitude between the two curves represented the clot strength at that time. From these results, the characteristic TEG trace and normal clot parameters were obtained when clotting was carried out in PBS or HPG-C18 at the experimental concentrations. We observed that HPG-C18 at concentrations of 0.01 and 10 mg/mL showed no difference in TEG trace from the PBS control, and the main parameters were in the normal range; this suggested excellent blood compatibility.

Table I. Values of Clotting Kinetics for Human Whole Blood Mixed with HPG-C18 Solutions at Different Concentrations ($n = 3$)

Sample	R (min)	K (min)	α (°)	MA (mm)
Normal range	5–10	1–3	53–72	50–70
PBS control	5.6 ± 0.14	2.0 ± 0.14	63.2 ± 0.99	61.2 ± 4.24
10 mg/mL HPG-C18	6.2 ± 0.25	1.9 ± 0.15	62.4 ± 2.68	60.4 ± 3.29
1 mg/mL HPG-C18	6.0 ± 0.32	1.6 ± 0.25	67.8 ± 3.09	62.4 ± 1.42
0.1 mg/mL HPG-C18	5.9 ± 0.37	1.8 ± 0.20	66.0 ± 2.69	59.0 ± 2.90
0.01 mg/mL HPG-C18	5.4 ± 0.26	1.6 ± 0.12	67.1 ± 1.90	62.4 ± 3.11

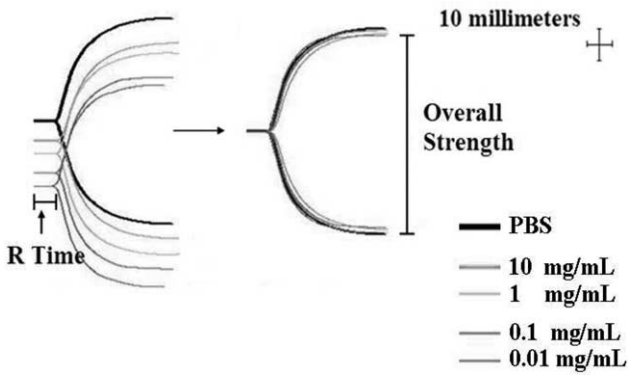

Figure 10. Representative TEG traces of whole blood coagulation in the presence of different concentrations of HPG-C18. [Color figure can be viewed in the online issue, which is available at www.interscience.wiley.com.]

From these results, we safely concluded that HPG-C18 had good biocompatibility and could be applied potentially in tumor therapy. Kainthan *et al.*[38] reported that HPG established a long circulation half-life, and the circulation time increased with increasing molecular weight. HPG generally accumulated in the liver and spleen and remained at least for 30 days, whereas there was very a low amount in the kidney because of the molecular weight. This suggested that HPG-C18 may also generally accumulate in the liver and spleen and may be potentially applied in liver cancer therapy.

CONCLUSIONS

An amphiphilic HPG (HPG-C18) composed of glycidol and 1,2-epoxyloctadecane monomers was synthesized through anionic ring-opening copolymerization. The obtained HPG-C18 formed large complex aggregates of many unimolecular particles. The complex aggregates showed good stability in aqueous solution. Because of its amphiphilic properties, HPG-C18 was used to load hydrophobic DTX, a clinical antitumor drug, to inhibit MCF-7 cell proliferation. Its blood compatibility was studied by hemolysis analysis, RBC observation, and TEG assay. These results indicate that HPG-C18 inhibited the MCF-7 cells effectively with good blood compatibility; this suggested potential applications in tumor therapy.

ACKNOWLEDGMENTS

This work was financially supported by the National Natural Science Foundation of China (contract grant number 31271019), the Natural Science Foundation of Guangdong Province (contract grant numbers 2014A030313361 and S2013010013452), and the Fundamental Research Funds for the Central Universities. The authors thank Yinglai Teng of Jinan University (China) for improving the English of this article.

REFERENCES

1. Zhang, X. D.; Zeng, X. W.; Liang, X.; Yang, Y.; Li, X. M.; Chen, H. B.; Huang, L. Q.; Mei, L.; Feng, S. S. *Biomaterials* **2014**, *35*, 9144.
2. Fujii, S.; Nishina, K.; Yamada, S.; Mochizuki, S.; Ohta, N.; Takahara, A.; Sakurai, K. *Soft Matter* **2014**, *10*, 8216.
3. Krishnamurthy, S.; Ng, V. W. L.; Gao, S. J.; Tan, M. H.; Yang, Y. Y. *Biomaterials* **2014**, *35*, 9177.
4. Murakami, M.; Saito, T.; Tabata, Y. *Acta Biomater.* **2014**, *10*, 4723.
5. Ding, Y.; Chen, W. L.; Hu, J. H.; Du, M.; Yang, D. *Mater. Sci. Eng. C* **2014**, *44*, 386.
6. Terreau, O.; Bartels, C.; Eisenberg, A. *Langmuir* **2004**, *20*, 637.
7. Yim, H.; Park, W.; Kim, D.; Fahmy, T. M.; Na, K. *Biomaterials* **2014**, *35*, 9912.
8. Nagaraj, K.; Ambika, S.; Rajasri, S.; Sakthinathan, S.; Arunachalam, S. *Colloids Surf. B* **2014**, *122*, 151.
9. Zhang, L.; Eisenberg, A. *J. Am. Chem. Soc.* **1996**, *118*, 3168.
10. Liu, Y.; Li, J. B.; Ren, J.; Lin, C.; Leng, J. Z. *Mater. Lett.* **2014**, *127*, 8.
11. Radowski, M. R.; Shukla, A.; Berlepsch, H. V.; Bttcher, C.; Pickaert, G.; Rehage, H.; Haag, R. *Angew. Chem. Int. Ed.* **2007**, *46*, 1265.
12. Paulus, F.; Steinhilber, D.; Welker, P.; Mangoldt, D.; Licha, K.; Depner, H.; Sigrist, S.; Haag, R. *Polym. Chem.* **2014**, *5*, 5020.
13. Kainthan, R. K.; Mugabe, C.; Burt, H. M.; Brooks, D. E. *Biomacromolecules* **2008**, *9*, 886.
14. Rossi, N. A.; Mustafa, I.; Jackson, J. K.; Burt, H. M.; Horte, S. A.; Scott, M. D.; Kizhakkedathu, J. N. *Biomaterials* **2009**, *30*, 638.
15. Luo, S.; Hu, X.; Zhang, Y.; Ling, C.; Liu, X.; Chen, S. *Polym. J.* **2011**, *43*, 41.
16. Kurniasih, I. N.; Liang, H.; Kumar, S.; Mohr, A.; Sharma, S. K.; Rabe, J. P.; Haag, R. *J. Mater. Chem. B* **2013**, *1*, 3569.
17. Deng, Y.; Saucier-Sawyer, J. K.; Hoimes, C. J.; Zhang, J.; Seo, Y. E.; Andrejecsk, J. W.; Saltzman, W. M. *Biomaterials* **2014**, *35*, 6595.
18. Zhao, L.; Xu, Y. H.; Akasaka, T.; Abe, S.; Komatsu, N.; Watari, F.; Chen, X. *Biomaterials* **2014**, *35*, 5393.
19. Zhang, W.; Zhou, X.; Liu, T.; Ma, D.; Xue, W. *J. Mater. Chem. B* **2015**, *3*, 2127.
20. Kainthan, R. K.; Janzen, J.; Levin, E.; Devine, D. V.; Brooks, D. E. *Biomacromolecules* **2006**, *7*, 703.
21. Shenoi, R. A.; Lai, B. F. L.; Imranulhaq, M.; Brooks, D. E.; Kizhakkedathu, J. N. *Biomaterials* **2013**, *34*, 6068.
22. Ma, D.; Zhang, H. B.; Tu, K.; Zhang, L. M. *Soft Matter* **2012**, *8*, 3665.
23. Lv, S. X.; Tang, Z. H.; Li, M. Q.; Lin, J.; Song, W. T.; Liu, H. Y.; Huang, Y. B.; Zhang, Y. Y.; Chen, X. S. *Biomaterials* **2014**, *35*, 6118.
24. Zhong, D. G.; Jiao, Y. P.; Zhang, Y.; Zhang, W.; Li, N.; Zuo, Q. H.; Wang, Q.; Xue, W.; Liu, Z. H. *Biomaterials* **2013**, *34*, 294.
25. Gohy, J. F.; Creutz, S.; Garcia, M.; Mahltig, B.; Stamm, M.; Jerome, R. *Macromolecules* **2000**, *33*, 6378.

26. Hong, H. Y.; Mai, Y. Y.; Zhou, Y. F.; Yan, D. Y.; Cui, J. *Macromol. Rapid Commun.* **2007**, *28*, 591.

27. Tian, W.; Wei, X. Y.; Liu, Y. Y.; Fan, X. D. *Polym. Chem.* **2013**, *4*, 2850.

28. Guo, J. T.; Hong, H.; Chen, G. J.; Shi, S. X.; Zheng, Q. F.; Zhang, Y.; Charles, P. T.; Todd, E. B.; Cai, W. B.; Gong, S. Q. *Biomaterials* **2013**, *34*, 8323.

29. Calejo, M. T.; Sande, S. A.; Nyström, B. *Expert Opin. Drug Deliv.* **2013**, *10*, 1669.

30. Koo, A. N.; Min, K. H.; Lee, H. J.; Lee, S. U.; Kim, K.; Kwon, I. C.; Cho, S. H.; Jeong, S. Y.; Lee, S. C. *Biomaterials* **2012**, *33*, 1489.

31. Wen, Y.; Meng, W. S. *J. Pharm. Innov.* **2014**, *9*, 158.

32. Yang, J.; Liu, Y.; Wang, H.; Liu, L.; Wang, W.; Wang, C. *Biomaterials* **2012**, *33*, 604.

33. Ma, Z. F.; Bai, J.; Wang, Y. C.; Jiang, X. *ACS Appl. Mater. Interfaces* **2014**, *6*, 2431.

34. Sarkar, K.; Chatterjee, A.; Chakraborti, G.; Kundu, P. P. *Carbohydr. Polym.* **2013**, *98*, 596.

35. Meng, S.; Liu, Z.; Shen, L.; Guo, Z.; Chou, L. L.; Zhong, W. *Biomaterials* **2009**, *30*, 2276.

36. Kainthan, R. K.; Gnanamani, M.; Ganguli, M.; Ghosh, T.; Brooks, D. E.; Maiti, S. *Biomaterials* **2006**, *27*, 5377.

37. Peng, H. T. *J. Biomed. Mater. Res. B* **2010**, *94*, 469.

38. Kainthan, R. K.; Brooks, D. E. *Biomaterials* **2007**, *28*, 4779.